Enhancing Chemiluminescence-Detection with Dark-Count Rate Optimization Strategies for SPADs in Conventional CMOS Technologies

Benjamin Saft[1], Alexander Zimmer[2], Maximilian Wiener[1], Mirjam Skadell[2], and Eric Schäfer[1]
[1] IMMS Institut für Mikroelektronik- und Mechatronik-Systeme gemeinnützige GmbH (IMMS GmbH), Ilmenau, Germany
[2] X-FAB Semiconductor Foundries GmbH, Erfurt, Germany
Email: {benjamin.saft, maximilian.wiener, eric.schaefer}@imms.de, {alexander.zimmer, mirjam.skadell}@xfab.com

***Abstract*— In this paper, we present a CMOS single-photon avalanche diode (SPAD)-based line sensor for the low-light detection of chemiluminescence in point-of-care in-vitro diagnostic applications, where lowest the dark-count rate (DCR) is paramount. Our work first presents the sensor chip architecture. Then we describe the layout optimization of the SPADs to minimize DCR while maintaining a high fill factor and a high photon detection probability (PDP). The sensor includes a high-density linear SPAD sensor array (192 lines), multiple SPADs and a shared quenching circuits per line, a hot pixel calibration to improve the signal-to-noise ratio (SNR), line-by-line pulse counting, adjustable measurement intervals, on-chip SRAM for data storage, ALU with memory-efficient bfloat16 encoding and interfaces via I2C and QSPI. Based on measurement results, we show that an optimal SNR for the low light application can be achieved by selectively deactivating certain SPADs, up to a high percentage (80%), depending on the DCR statistics of the sensor.**

I. Introduction

Chemiluminescence is widely used as a diagnostic tool, e.g. in clinical laboratory equipment [1]. Compared to other in-vitro diagnostic (IVD) detection methods such as fluorescence, chemiluminescence has various advantages: no light source or optical filters are required to trigger and discriminate the signal of interest, and background signals can be minimized easily by using dark environments. This makes chemiluminescence an interesting detection system for cost-sensitive point-of-care testing. In [2], Sandetskaya *et al.* present a chemiluminescent immunoassay in a lab-on-a-chip format with high cost-saving potential in comparison to the conventional laboratory readers. The disadvantage of chemiluminescence is that the emitted light intensity is extremely low, especially if the required limit of detection should meet that of other detections methods.

Photomultiplier tubes (PMT) are widely employed as detectors for low-light sensing in in-vitro diagnostics, bioanalytical and biomedical applications. They provide high sensitivity and low dark-count rates (DCR). Micro PMTs that would also fit into point-of-care devices, such as the H12406 from Hamamatsu [3], achieve a high sensitivity of approximately 1×10^{-2} cps/(pW (µm)^2) and a low DCR of approximately 1×10^{-4} cps/(µm)^2. The disadvantage of PMTs are their high costs for the detector itself as well as the need for scanning mechanics if spatial resolution is required. Single photon avalanche diodes (SPAD) are considered a promising alternative to PMTs [4]. Their monolithic integration with readout electronics allows for low-cost mass production, miniaturization, and imaging without scanning mechanics.

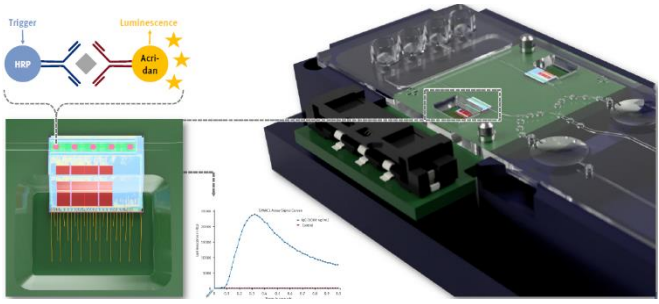

Fig. 1. Assembly consisting of the sensor PCB and the microfluidic chip. The chemiluminescence reaction is happening directly in the microfluidic channel located directly above the SPAD array of the sensor.

Based on these considerations, we developed a SPAD-based line sensor in a commercial CMOS technology for integration into microfluidic cartridges [5], as shown in Fig. 1.

The sensor was designed to measure light emission inside a microfluidic channel without any optics. The 192 lines provide sufficient spatial resolution inside the channel, enabling the distinction of up to ten spots with immobilized capture molecules sensitive to various biomarkers. We used the sensor to readout a chemiluminescence immunoassay for the rapid detection of the life-threatening inflammatory cytokine release syndrome (CRS) [6].

In this paper, we present our optimization strategy to reduce DCR of the SPAD devices while maintaining a high photon detection probability (PDP). We identified and studied twelve different SPAD variants, which we employed in our line sensor IC. We present the statistical measurement data for a subset of the variants. Based on these results, we derived a hot-pixel classification strategy that leads to an optimal signal-to-noise ratio (SNR) for our application.

II. Architecture of Sensor IC

The sensor IC consists of a SPAD array that covers an area of approximately 3.4 x 0.35 mm², divided into 192 sensor rows running along the channel's length, see Fig. 2. This configuration allows for spatially resolved recording of the temporal sequence of the light emission within the channel.

Each row features 10 or 20 SPADs, depending on the SPAD variants, closely packed with minimal spacing, as shown in Fig. 3. In contrast to other published biomedical sensors (e.g. [7], [8]), our emphasis lies on achieving maximum fill factor and optical sensitivity. Hence, all auxiliary circuitry, including the quenching circuitry, is positioned alongside of the sensor array. This circuitry includes switches for enabling/disabling each SPAD individually, a common row active quenching circuitry with two programmable analog timers for quenching and charging

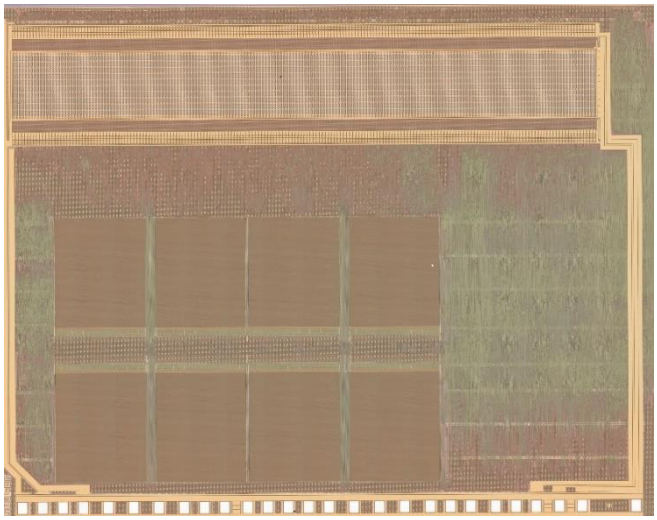

Fig. 2. Micrograph of the CMOS SPAD-based line sensor ASIC.

Fig. 3. Detailed view of the row architecture/layout with ten active SPADs plus two dummy SPADs per row. Here: layout variant BF.

time. The quenching circuit is shared among all enabled SPADs of the row. There is an optional pull-up current source to prevent DCR increase due to leakage in the quenching circuit. The row architecture also incorporates a digital after-pulse filter and finally a 16-bit common counter.

Besides the sensor array, the IC includes I2C and QSPI interfaces, 64 kB of SRAM for buffering the measurements of the line counters, a programmable sequencer for control of the image capturing, and an ALU which applies a memory-saving bfloat16 encoding to the captured sensor data.

The chip incorporates additional means to enhance effective sensitivity. For low light chemiluminescent detection its crucial to achieve the lowest possible DCR while maintaining a high light sensitivity. Therefore, dedicated logic and algorithms are employed to selectively deactivate a certain percentile of SPADs determined by the DCR statistics of the sensor. The method works as follows: Initially, the dark-count rates of each SPAD in the sensor array is measured individually and a histogram is created. Subsequently, a certain percentile of the poorest-performing SPADs (screamers) is selected and marked in a deactivation map. This map is loaded into the sensor and employed for any further measurements. The key parameter for this is the switch-off-threshold above which the remaining SPADs are switched off. This is discussed further in the Statistics section.

III. Layout Optimization of SPADs

The effectiveness of the SPAD switch-off-threshold is closely related to the inherent quality of the SPADs. Therefore, SPAD layout optimization is essential for improving overall DRC performance.

The chip was designed using the commercial 0.18-µm CMOS process XH018 from X-FAB. Within this process two non-isolated basic SPAD devices, dspada and dspb, are available. The reduction of the dark-count rate and the increase of the photon detection efficiency are the main challenges for the layout optimization, which is focused especially on the periphery of the SPAD devices. All these layout adjustments were made to create a layout with a defined pitch of 18.87 µm to interchangeably place different variations of the SPADs in the sensor array.

The modification of the DCR was first realized with layout changes in the virtual guardring, due to differences between

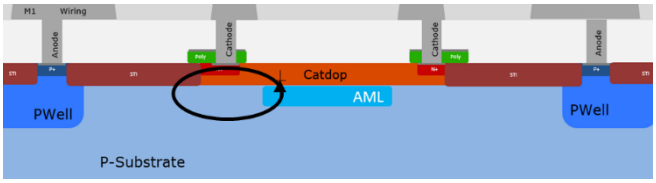

Fig. 4. XH018 dspada – first generation SPAD from X-FAB. The peripheral area is not optimized. Especially AML to STI spacing is

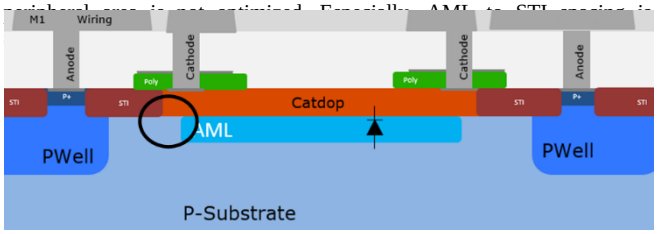

Fig. 5. XH018 dspb – design improved SPAD. One optimization leads into the virtual guardring design of the AML-STI spacing.

the dspada (Fig. 4) and dspb (Fig. 5) as well as the distance of the non-sensitive area in the periphery. A different spacing of the avalanche multiplication layer (AML) is used towards the shallow trench isolation (STI) edge. This already leads to a significantly different virtual guardring architecture and impact on DCR [9]. Second, the increased anode-to-cathode distance, shown as PWell-to-Catdop distance in Fig. 6, similarly improves the DCR. In addition, an additional diode (guardring) was placed around the SPAD device outside of the anode contact. On the one hand, this further reduces the fill factor, but on the other hand, it also serves the purpose of sucking the charge carriers from the surroundings.

To also improve the sensitivity, we optimized the layout of the SPADs with respect to the fill factor. For this, the

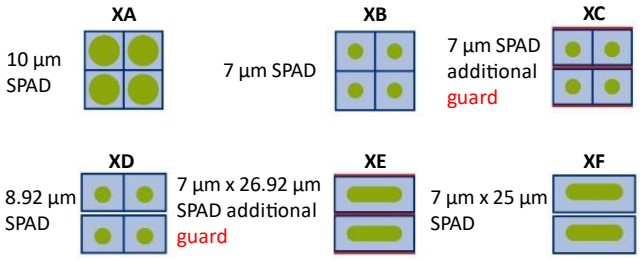

Fig. 7 Six layout variants (encoded with A-F as second letter) for each device architecture ("dspada" architecture encoded with A, "dspb" architecture encoded with B as first letter) have been realised. Next to sizes, we adapted also AML-STI to fulfil the criteria of a fixed pitch of 18.87 µm.

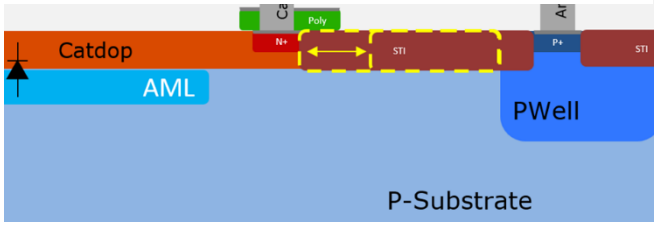

Fig. 6. Catdop distance to PWell as one of the layout parameters. By changing this value, the STI width between anode and cathode has been changed.

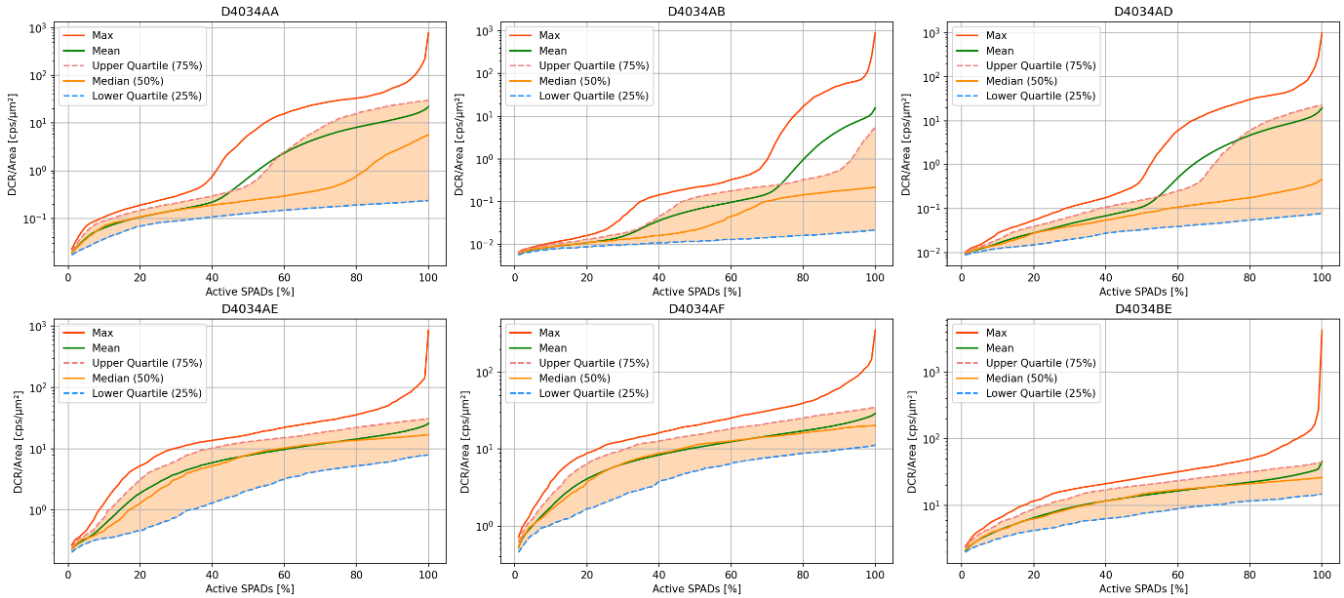

Fig. 8. Area-related DCR distribution over the percentile of active SPADs for six different layout variations at 25°C.

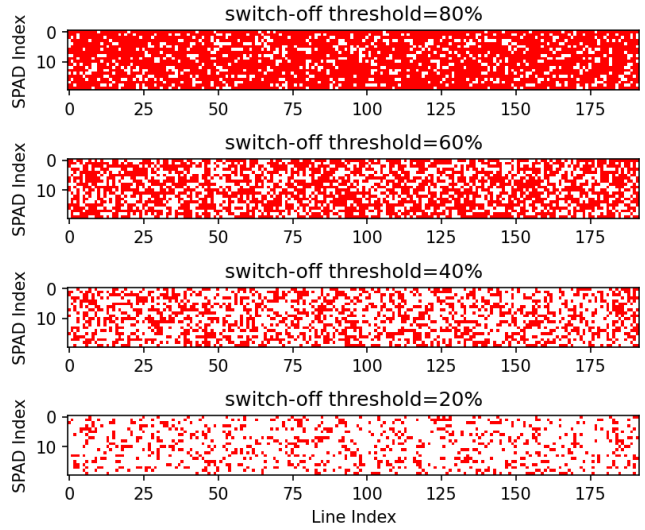

Fig. 9. SPAD masks for different switch-off thresholds (red = deactivated).

avalanche active area is inflated or even an asymmetric version has been used with a width of double the pitch is employed. In summary, six different parameterized designs are used for each SPAD architecture (Fig. 7). In addition to the basic mechanism of changing the parameters in terms of fill factor, PDP or DCR, the focus was also on the uniformity and distribution of the DCR.

IV. Statistical Measurement Results

A preliminary analysis of the specific detectivity for all twelve device variants was performed. Six variants with low noise and/or high PDP were pre-selected and used for further statistical analysis: AA, AB, AD, AE, AF, and BE. The first letter represents the SPAD device type (“A” for dspada and “B” for dspb). The second character indicates the layout variant (see Fig. 7).

To compare the layout variants of the SPADs and find the optimal switch-off-threshold (screamer classification), we analyzed the area-related DCR distribution across the active SPAD percentiles for the most promising chip types, see

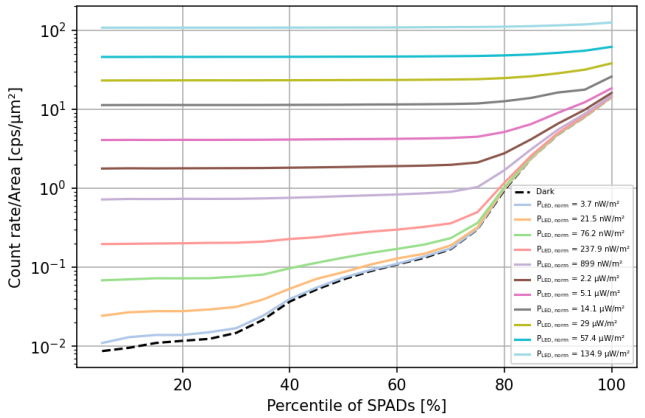

Fig. 10. Area-related SPAD count rate vs. the percentile of SPADs for the AB device at different illumination levels at 25°C. It clearly can be seen that it is necessary to switch off a major amount of the total SPAD devices to measure low irradiance levels.

Fig. 8. The SPAD percentile signifies that all SPADs with a higher percentile than the selected value, exhibiting a higher DCR, are deactivated. Hence the switch-off threshold is defined as one minus the selected percentile. The DCR varies over more than three decades for different switch-off thresholds. From this it follows that it can be advisable to use a high switch-off-threshold when the application only shows a very low irradiance. As stated in [10], DCR for SPADs usually follows a log-normal distribution. This is valid for the types E and F. Interestingly, types A-D exhibited distributions distinct from a log-normal distribution.

When employing a high switch-off threshold, maintaining adequate spatial resolution becomes crucial for the chemiluminescence detection in the fluidic channel. Subsequently, we measured the SPAD deactivation masks for various switch-off thresholds to ensure a randomly spatial distribution of deactivated SPADs, see Fig. 9. As it can be seen even with high thresholds of 80% a sufficient special distribution along the sensor lines is maintained.

We investigated the performance of the devices under low light conditions, measuring SPAD count rates at various irradiance levels for chip type AB (see Fig. 10). A blue homogeneous 460 nm LED light source was employed for illumination. The figure illustrates that the switch-off threshold does not matter at higher illuminance levels. Yet, at very low irradiance levels, it is beneficial to deactivate significant portions of the SPADs to prevent the signal from getting lost in the noise.

Based on these measurements we calculated the SNR as

$$SNR = \frac{PDE\ \Phi_P\ t}{\sqrt{(PDE\ \Phi_P + 2DCR)t}} = \frac{(MCR - DCR)t}{\sqrt{(MCR + DCR)t}},$$

where Φ_P is the rate of photons per second and PDE is the photon detection efficiency [11]. Since Φ_P cannot be measured the measurement count rate MCR is used. It is calculated as $MCR = PDE\ \Phi_P + DCR$. To get an intuitive measure for the SNR at different integration times we plotted

$$\frac{SNR}{\sqrt{t}} = \frac{MCR - DCR}{\sqrt{MCR + DCR}}$$

in Fig. 11. The chart shows that at medium-low intensities around 1 µW/m², a threshold of approximately 70% is enough to preserve the maximum SNR. However, in very low-light conditions below 100 nW/m², it is advantageous to keep only around 20-30% of the top-performing SPADs active to maintain the highest SNR with acceptable spatial resolution. If you would keep the previous threshold of 70%, the DCR would be significantly worse (up to 10 times).

These findings indicate that employing the common approach of a fixed, relatively high cutoff threshold is effective for medium to high incident light levels. However, in low-light conditions where count rates approach the DCR, it is recommended to use a considerably lower cutoff threshold.

V. Conclusions

We showed that a combination of SPAD device optimization, a flexible sensor IC architecture, and hot-pixel calibration based on statistical evaluation can lead to very high sensitivity and low DCR. We achieved a DCR of approximately 1×10^{-2} cps/(µm)^2 which is only about two orders of magnitude above the DCR of PMTs. We kept only 20% of the SPADs with the lowest DCR active which results in high SNR even for very low chemiluminescence light emissions. Due to an equal distribution of DCRs over the array, such a massive deactivation of SPADs can be seen as loss of spatial resolution. For our application with up to ten light-emitting spots in a microfluidic channel, we do not expect any drawbacks from switching off 80% of all SPADs.

Further research will include the effect of temperature of the DCR statistics as well as an investigation of the underlying statistical effects we observed for small SPADs, e.g. the strong divergence between mean and median for high percentiles.

Acknowledgment

This work has been carried out in the project KODIAK which was funded as part of the European Union's response to the COVID-19 pandemic through the European Regional Development Fund (ERDF-OP 2014-2022) under the references 2021 FE 9127 and 2021 FE 9129.

REACT-EU – Als Teil der Reaktion der Union auf die COVID-19-Pandemie finanziert.

EFRE EUROPA FÜR THÜRINGEN
EUROPÄISCHER FONDS FÜR REGIONALE ENTWICKLUNG

EUROPÄISCHE UNION

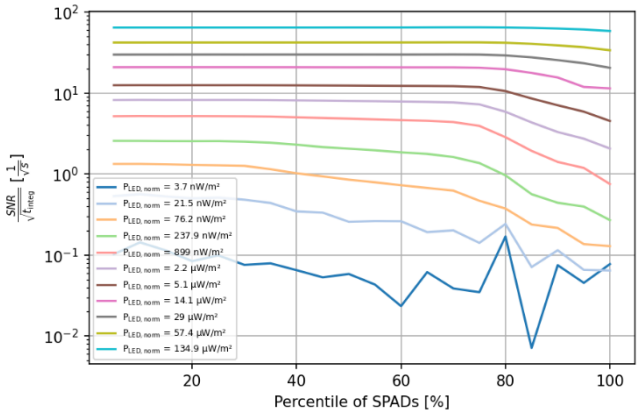

Fig. 11. Effective measurement signal to dark signal ratio vs. the percentile of SPAD utilization for different excitation light powers.

References

[1] C. Dodeigne, "Chemiluminescence as diagnostic tool. A review," Talanta, vol. 51, no. 3, pp. 415–439, Mar. 2000.J. Clerk Maxwell, A Treatise on Electricity and Magnetism, 3rd ed., vol. 2. Oxford: Clarendon, 1892, pp.68–73.

[2] N. Sandetskaya *et al.*, "An integrated homogeneous SPARCLTM immunoassay for rapid biomarker detection on a chip," Analytical Methods, vol. 11, no. 19, pp. 2542–2550, 2019, doi: https://doi.org/10.1039/c9ay00198k.

[3] "Micro PMT photon counting head H12406," Hamamatsu Photonics. Online: https://www.hamamatsu.com/eu/en/product/optical-sensors/pmt/micro-pmt/H12406.html (accessed Nov. 30, 2023).

[4] M. Caccia *et al.*, "Silicon Photomultipliers and SPAD imagers in biophotonics: Advances and perspectives," Nuclear Instruments and Methods in Physics Research A, vol. 926, pp. 101–117, May 2019, doi: https://doi.org/10.1016/j.nima.2018.10.204.

[5] A. Zimmer *et al.*, "SPAD-based line sensor IC for chemiluminescence assays in microfluidic channels," to be presented at *Conference of Science & Technology for Integrated Circuits (CSTIC)*, Shanghai, China, 2024.

[6] M. Scholles *et al.*, "KODIAK: Components and modules for improved optical diagnostics", *MikroSystemTechnik Congress 2023*, Dresden, Germany, 2023.

[7] M. A. Al-Rawhani *et al.*, "Multimodal Integrated Sensor Platform for Rapid Biomarker Detection," in IEEE Transactions on Biomedical Engineering, vol. 67, no. 2, pp. 614-623, Feb. 2020.

[8] V. F. Annese *et al.*, "The Multicorder: A Handheld Multimodal Metabolomics-on-CMOS Sensing Platform," *2019 IEEE 8th International Workshop on Advances in Sensors and Interfaces (IWASI)*, Otranto, Italy, 2019, pp. 130-135.

[9] C. Veerappan, "Single-Photon Avalanche Diodes for Cancer Diagnosis," 2016, doi: https://doi.org/10.4233/uuid:7db13e84-9ced-4c9c-94fa-8c2a14ad6679.

[10] P. W. R. Connolly *et al.*, "Hot pixel classification of single-photon avalanche diode detector arrays using a log-normal statistical distribution," Electronics Letters, vol. 55, no. 18, pp. 1004–1006, Sep. 2019, doi: https://doi.org/10.1049/el.2019.1427.

[11] Hamamatsu Photon Counting SNR Simulator, Online: https://www.hamamatsu.com/eu/en/resources/interactive-tools/photon-counting-snr-simulator.html